Antennas for underground Communications

EXECUTIVE SUMMARY

Written by Germán León, Project Manager of "Antennas for Underground Communications"

1 BACKGROUND AND PROJECT OBJECTIVES

Lava caves are long subterranean tubes generated by lava flows. On the Moon, they are stable structures much bigger than Earth caves, with a width between 50m and 300m and several kilometers long. The entrance to these caves is a collapse, perpendicular to the tube, called a skylight, around 60m long. Lunar lava caves could be used potentially as human settlements, due to their protection against micrometeorite bombing and temperature stability. These Lunar caves are still unexplored and different approaches have been proposed to discover these tubes. Their proposal is to have a small fleet of robots descend into the cave, from the skylight (or pit). Inside the lava cave, this fleet will deploy an ad-hoc communications network which allows the scientific data from the interior to be transmitted from the cave to the Moon surface.

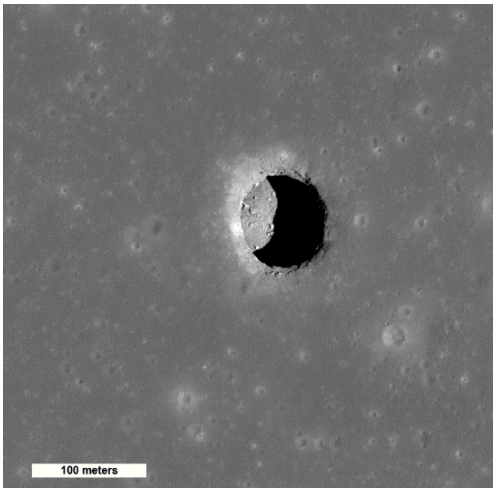

Figure 1. The Marius pit is about 34 meters deep and 65 by 90 meters (approximately 213 by 295 feet) wide. Credits: NASA/GSFC/Arizona State University.

This project pursues the following objectives:

- To provide of model of the propagation of signals within natural caves.
- To design an antenna that can support and maximize data transmission to the entrance of the cave.

Moreover, the antenna shall be tested both in an antenna measurement facility and in a natural cave.

2 PROPAGATION MODELS

2.1 GEOMETRICAL OPTICS APPROACH

Into the caves, a image model has been applied considering four images, to account for simple reflections on ground, ceiling, and walls. The geometrical model was simplified by considering all surfaces to be flat and smooth. Figure 2 show some results in La Corona. The mean received power is mainly determined by the combination of the direct and ground reflected paths and will be close to the prediction given by the two-ray propagation model, while reflections on walls and ceilings are the responsible for fading.

Frequency responses were also measured under LoS conditions in both Naturalistas cave and La Corona at different distances between the transmitter and the receiver, and measurements were processed to obtain the channel impulse response. Figure 3(a) shows the six impulse responses measured in La Corona. It can be seen that there is a clear dominant path for all the measured positions and the relevant presence of reflection on walls after this main path. The dominant path will be the sum of the direct path and the ground reflected path, since this cannot be resolved due to its proximity to the direct one. Figure 3(b) shows the estimation given by the image model. No multiple reflections on walls have been included in the model. Due to their low amplitude these

effects are not relevant when estimating the RSSI, but they will be in the estimation of the wideband parameters of the channel (delay spread, coherence bandwidth).

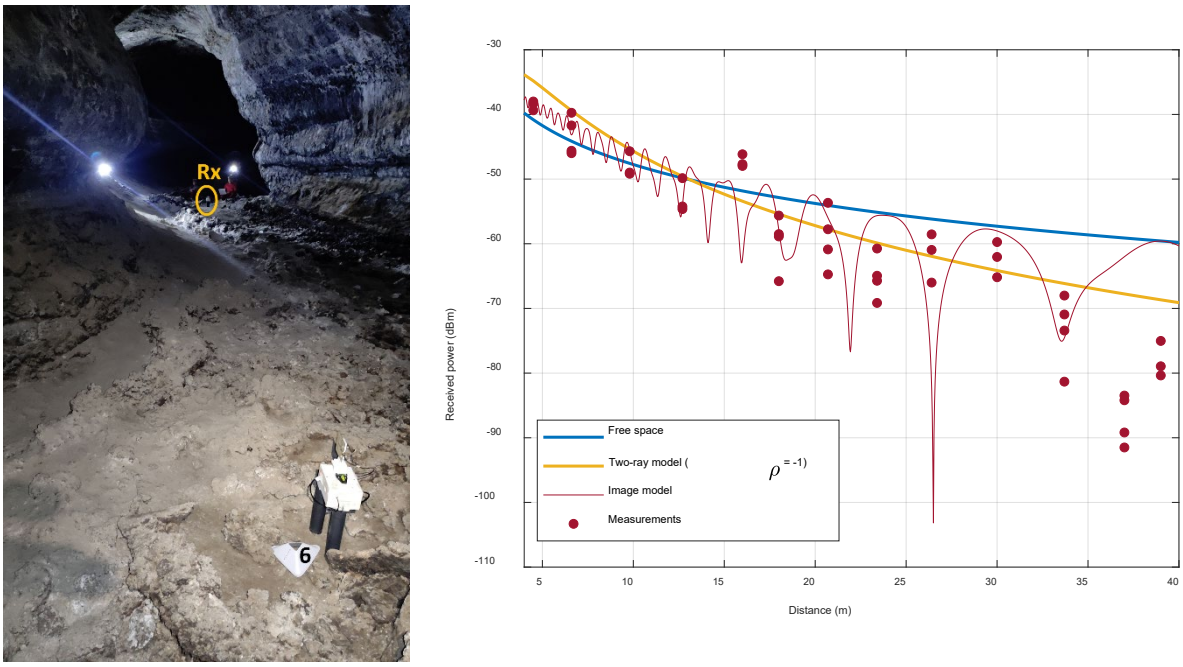

(a) (b)

Figure 2. *Measurements in La Corona lava tube. (a) measurement set-up, (b) comparison of measurements and model.*

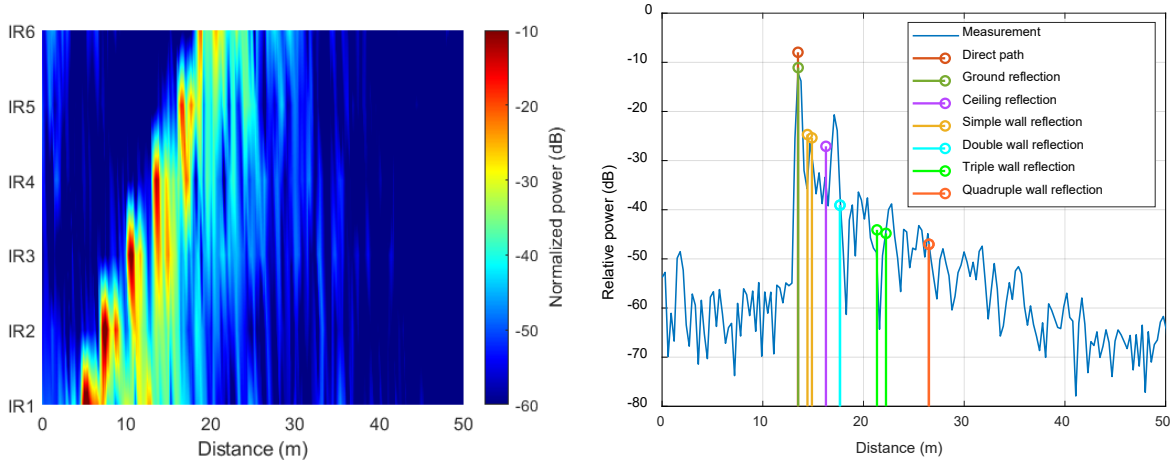

(a) (b)

Figure 3. *Measurements in La Corona lava tube. (a) measurement set-up, (b) comparison of measurements and image model.*

2.2 PHYSICAL OPTICS MODEL

Geometrical optic is a fast method but has limitations:

- It is an asymptotic method that works better the higher the frequency.
- There are versions for reflection in curved ground, which require focal length changes that are easy to calculate only in very simple geometries
- It does not incorporate the effect of diffraction.

To solve these limitations, Physical Optics model has been developed which consists of calculating the electromagnetic field scattered from electric and magnetic currents from the surface (floor, walls or ceiling) generated by the transmitted antenna.

This method has been to study the increment of losses due to obstacles (boulders). In Figure 4, two simulations are shown for an obstacle with width 10m and two different heights. At some distance, the received power is similar in all cases but increasing the height of the obstacle implies greater attenuation just after the obstacle and also more distance after the obstacle before the signal is recovered. This effect was simulated with more detail, and the results are shown Figure 5.

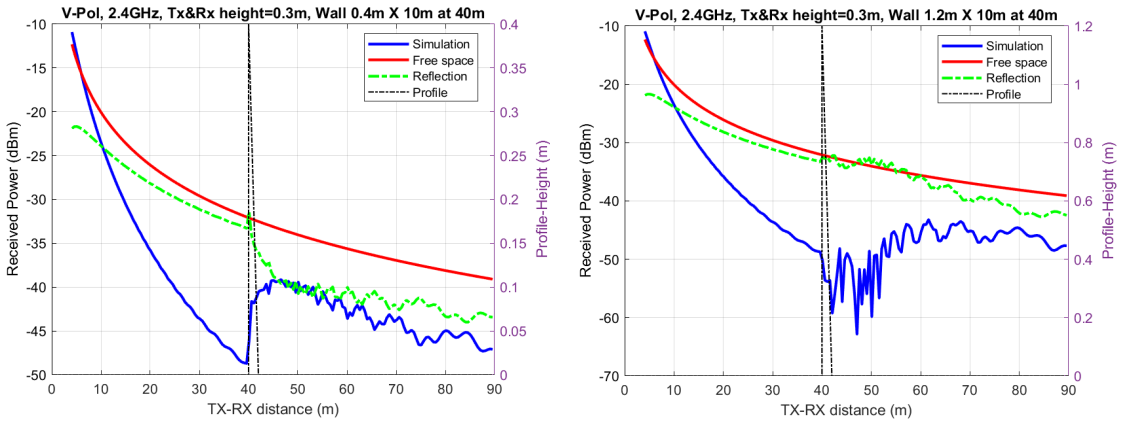

Figure 4. *Obstacle of 10m (width) at 40m of the transmitter for vertical polarization and 2.4GHz for 0.4 and 1.2m of heigth.*

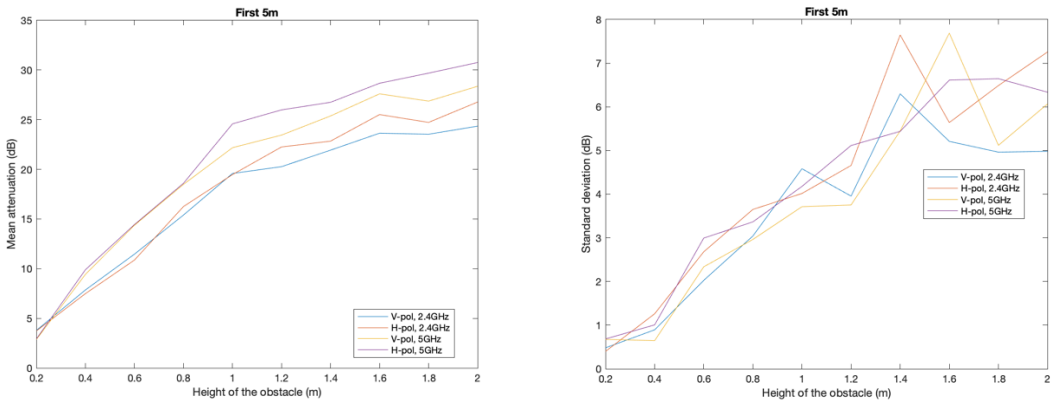

Figure 5. *Mean attenuation (left) and standard deviation (right) for an obstacle at 40m of the transmitter different heights for distances between 1 and 5m.*

In Figure 5, it can be seen that increasing the height of the obstacle increases both the mean attenuation and the variability. As an example, for 1m, the mean attenuation is about 20dB with a standard deviation of 4dB in the first 5m after the obstacle. It can be seen that the results are similar with different polarization and frequency, with slightly worst results for horizontal polarization and 5 GHz.

3 REQUIREMENTS CONSOLIDATION

The best strategy to explore a lava tube is *mobile ad-hoc network* (known as MANET). In MANETs, all the robots act as relays, so a multi-hop connectivity is established. That is, data packets travel from one robot to another until they arrive the base. It can fulfill our objective, but two main disadvantages have to be taken into account. On the one hand, the data packets can arrive from different points, with different delays and different bit errors. Some approaches can be found to overcome this issue, but they are out of the scope of the present project. On the other hand, a strong coordination between robots shall be as follows: all the robots shall be connected at every moment and for every event; for example, exploration in the deep part of the cave and robot refilling have to be deeply studied.

In this scenario, omnidirectional antennas are the best option, as opposed to medium gain antennas, in order to give flexibility to the exploration job.

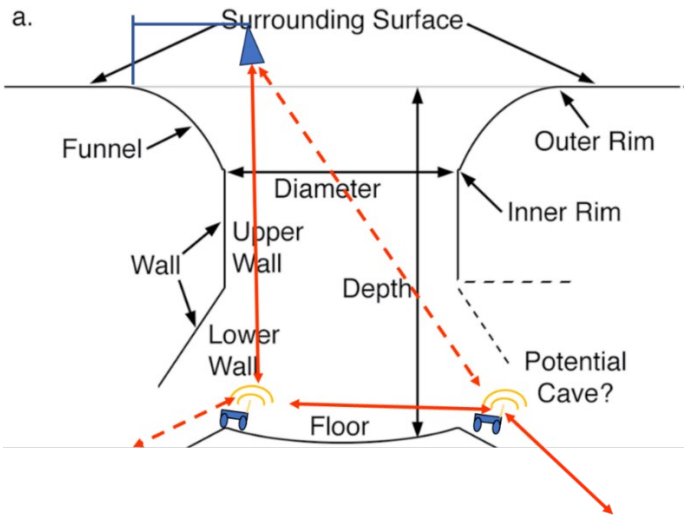

Figure 6. Ad-hoc mobile communication network. a) Top view[1].

In this activity, some systems requirements have been identified:

- The network must provide and maintain essential services under adverse conditions as well (resilience requirement).
- Mobile nodes facilitate the deployment and redeployment of the network, making it possible to tailor the network topology to the incident zone conditions. Moreover, the positions of the nodes can be modified to improve network performance (mobility

[1] Extracted from: Wagner, R. V., & Robinson, M. S. (2022). Lunar pit morphology: Implications for exploration. *Journal of Geophysical Research: Planets*, 127, 2022JE007328. https://doi.org/10.1029/2022JE007328

requirement).

- Any robot shall act as a communication relay.
- The communication subsystem (CSS) shall have an algorithm capable to monitor the link quality.

***Table 1**: Proposed functional requirements for the communication subsystem*

ID	Statement	SoW ID
COM-FUN-010	The robot fleet shall communicate using the S-band	REQ-010
COM-FUN-020	The CSS shall have a bandwidth of 100MHz at least	REQ-020
COM-FUN-030	The data rate, at the gateway shall be greater than 25 Mbps	REQ-090
COM-FUN-040	The fleet shall be able to establish a communication link between the explorer and the gateway using four hops.	REQ-140
COM-FUN-050	The data rate of a single hop shall be greater than 100 Mbps	REQ-090 & REQ140
COM-FUN-060	The robot fleet shall be able to communicate bidirectionally in a decentralized many-to-many network configuration	NA
COM-FUN-070	The CSS shall be robust against multipath interference.	NA
COM-FUN-080	The CSS shall be able to exchange information in a best effort manner depending on the distance and line of sight conditions.	NA
COM-FUN-090	The CSS shall have a power dynamic control	NA
COM-FUN-100	The sensitivity of the CSS shall be below -71 dBm	NA
COM-FUN-110	The CSS shall have an algorithm capable to monitor the link quality	NA

***Table 2.** Proposed functional and non-functional requirements for an omnidirectional circular polarized antenna*

ID	Statement	SoW ID
ANT-FUN-010	The antenna shall be matched at the same frequency band that the CSS, at least, with the same bandwidth	REQ-010,020
ANT-FUN-020	The antenna shall be circular polarized	REQ-040
ANT-FUN-030	The antenna shall have a realized gain greater than 0 dBi in the whole horizontal plane.	REQ-030
ANT-FUN-040	The antenna shall have a realized gain greater than 0 dBi in the vertical plane, between -30º and 30º.	NA
ANT-NFun-010	The mass of the antenna shall be below 120g	REQ-060
ANT-NFun-020	The diameter of a sphere involving the antenna set shall be below 20 cm	REQ-070
ANT-NFun-030	The antenna shall operate between -20^0 and 60^0C	REQ-080

4 ANTENNA DEVELOPMENT

4.1 ANTENNA DESIGN

The optimized pagoda antenna has been placed inside a protective radome with a mechanical support structure (see Figure 13), using three slots to fit the antenna together with the radome. It has been optimized once more to re-adjust its performance accordingly.

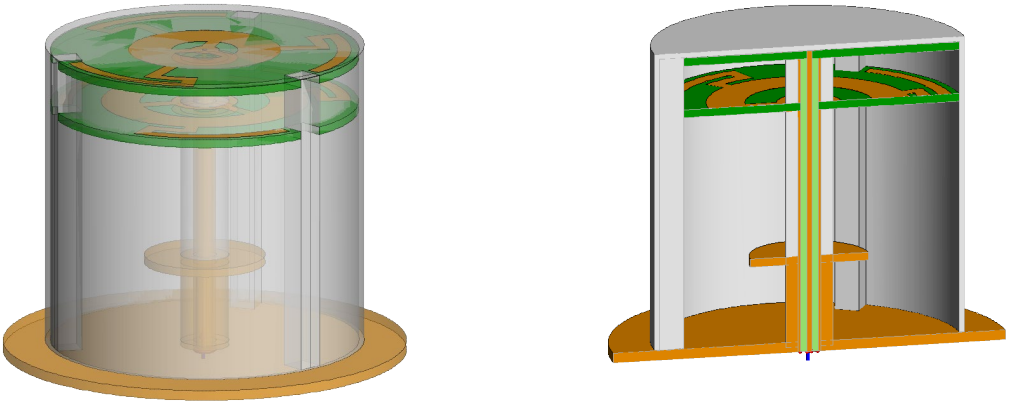

Figure7. *Antenna RF simulation model*

The above Pagoda antenna has been simulated using FEKO software from 2.4 to 2.5 GHz. Note that the substrate thickness has been increased in order to obtain better adaptation of the S11 Parameter.

The S-parameter and radiation results are presented in Figure 14 and Figure 15 respectively.

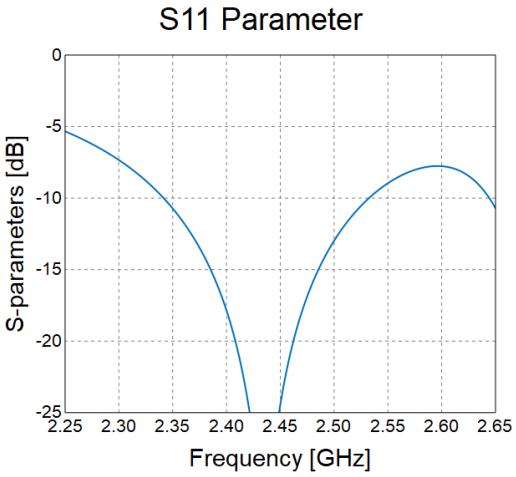

Figure 8*. Antenna RF S-Parameter results*

Figure 9. *Antenna radiation performance at 2.40 GHz (a) side view and (b) top view, at 2.45 GHz (c) side view and (d) top view, and at 2.50 GHz (e) side view and (f) top view*

4.1.1 Mechanical design of the selected antenna

The antenna's mechanical design is shown in Figure 10, and its mechanical properties in Table 5.

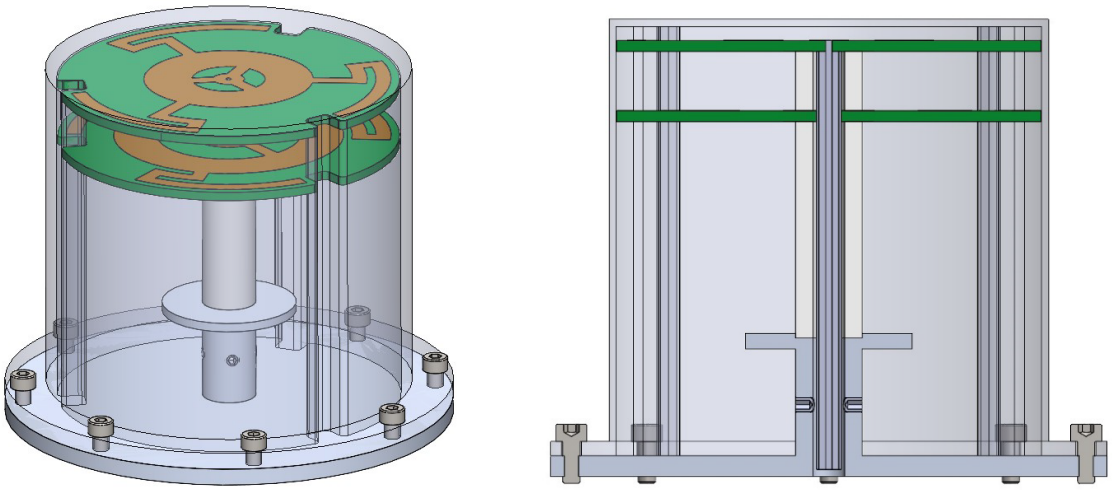

Figure 1. *Mechanical model of the antenna*

Table 3. *Mechanical properties*

Parameter	Value
Width (Ø)	65 mm
Height (H)	65 mm
Disc separation	9 mm
Inner wire diameter	0.91 mm
Dielectric diameter	3.58 mm
Dielectric material	Teflon
Substrate height	1.575 mm (62 mils)
Substrate material	Duroid 5880
Substrate dielectric constant	2.2
Radome thickness	1 mm
Radome material	PEEK
Radome dielectric constant	3.3
Antenna weight	< 120 g

4.2 ANTENNA STRUCTURAL ANALYSIS

In this section an executive summary of the structural analysis is presented.

4.2.1 Mechanical concept

The mechanical concept for the antenna comprises three elements:

- The baseplate
- The assembly composed by the cable, the disks and the PEEK cable protector
- The radome

The cable assy is attached to the baseplate through the lowest of the PEEK protectors using hardened Araldite 138 AM glue and then this protector is attached to the cable with this same glue. Regarding strength analysis, the limiting union is the attachment between the base and the

PEEK protector. This union was dimensioned to have enough resisting surface to cope with the random vibration. The disks are assembled on the cable by welding using copper.

A Finite Element Model was built following the .stp file provided by the EOSOL team. Although global dimensions were used, the complex geometrical shapes were substituted by flat surfaces, except for the cable that was represented as a solid 3D mesh, everything resulting in a simple Patran geometry (Figure 11). The unions were modelled using two RBE2 MPCs between the joint areas with a CBUSH to recover loads between the RBE2s.

The antenna cable is aligned with Y direction and X and Z define the plane in with both the disks and the baseplate are contained

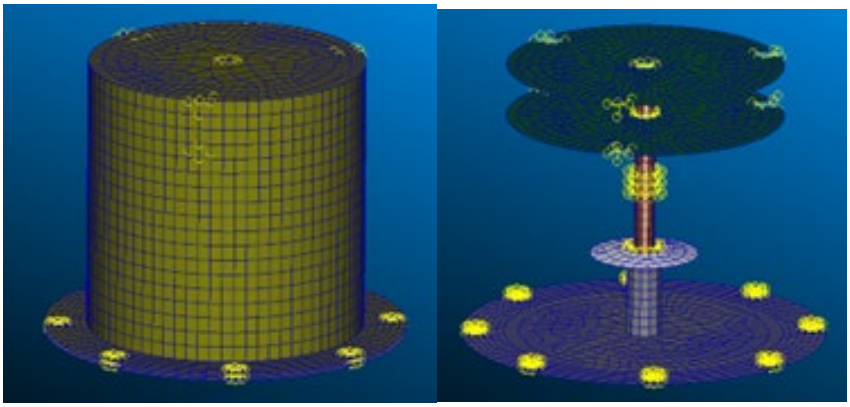

***Figure 11**. Pictures of the antenna assembly, FEM.*

4.2.2 Analysis and results

At this stage, a normal mode analysis and random analyses were performed. For the eigenmodes, the lower limit of 140 Hz was set (as usual with similar hardware). For the random analysis NASA GEVs were applied, as there is still no rover information, and those levels (14.1 g rms) are quite conservative for new designs.

4.2.2.1 Normal modes analysis

The first normal mode with MEM above 5% is at 280.5 Hz, which is double the imposed limit.

4.2.2.2 Random vibration analysis

Margins of safety for Random 3σ stress and force values were obtained. They are presented in the following Table 6 and Table 7. As there is not going to be testing at this stage, factors of safety of 1.6 and 2.0 were applied, on top of a model uncertainty factor of 1.2. This implies a safety factor over the calculations of 2.4.

***Table 4:** Margins of safety for the different materials of the antenna*

Material	Al6082	Teflon	Duroid	PEEK	Copper
Yield Str [Pa]	2.50E+08	1.50E+07	2.70E+07	5.00E+07	2.20E+08
U. Str [Pa]	2.90E+08	1.50E+07	2.70E+07	5.00E+07	2.76E+08

Rnd Horz stress [Pa]	1.03E+07	5.60E+06	1.90E+06	6.20E+06	1.53E+07
Rnd Vert. Stress [Pa]	3.30E+06	2.50E+06	5.01E+06	1.70E+06	4.75E+06
MoS,y	11.64	0.40	1.81	3.20	6.49
MoS,u	10.73	0.12	1.25	2.36	6.52

Table 5: *Margins of safety for the different joints of the antenna.*

Union	Glue 12	Weld 25	Weld26	Glue 23
Area [m2]	1.66E-05	7.23E-06	7.23E-06	3.62E-05
Material	A138	Cu	Cu	A138
Strength [Pa]	6.00E+06	2.20E+08	2.20E+08	6.00E+06
Load Horiz [N]	1	9.4	3.9	13.8
Load Vert [N]	28.3	13.3	13.4	28.3
epsjoint	0.75	0.1	0.1	0.7
Max strss (L/A) [Pa]	1.71E+06	1.84E+06	1.85E+06	7.82E+05
MoS joint	0.10	3.98	3.94	1.24

The margins are positive and mostly quite large. There are two points to keep track of in the next stages of the design: stress on the inner parts of the PTFE cable (margins are positive but close to zero) and the joint between the PEEK protector and the base. The first should be kept under check for the future. However, that is a conservative number as the area of the union that leads to this stress is slightly under-sized in the model in order not to provide excessive stiffness through the RBE2. More detailed modelling in the future should bring this value up. Regarding the second joint, if it is needed, the joint area could be further increased but at this point due to the very high safety factors it is not believed to be necessary.

Therefore, the conclusion is that, from a structural point of view, the design will be able to accomplish the mission and could proceed to next phase of design

4.3 Antenna Gain Test

The Field of View (FoV) of the antenna shall be a full 360° in azimuth and +/-30° from the horizontal (at least). The antenna shall be circular polarized (axial ratio < 3 dB) and shall have a gain of 0dBi in the FoV.

a) b)

Figure 12. a) QM_01 in the anechoic chamber; b) Schematic representation of the antenna under test, together with the definition of the reference system

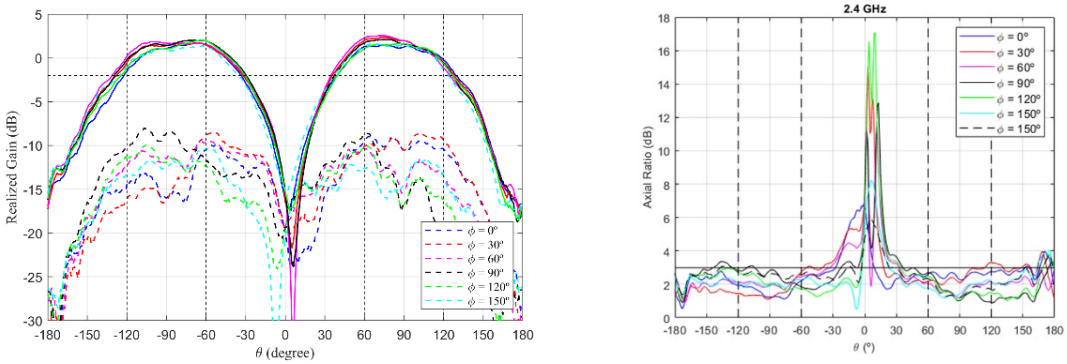

a) b)

Figure 13. Measured realized gain of the QM1 at 2.4 GHz (a) and axial ratio (b) for different φ cuts.

First, the measured gain is larger than 0 dB in the angular ranges with θ between -90º and -60º, and between 60º and 90º, which meets the ANT-FUN-040 requirement. On the other hand, the gain is larger than 0 dB in the $\theta = 90^o$ and $\theta = -90^o$ for all the φ cuts, which satisfies the ANT-FUN-030 requirement. In addition, the negligible differences found when comparing the different φ cuts, indicate that the manufactured antenna exhibits revolution symmetry with respect to the z-axis, as expected.

4.4 ANTENNA TVAC TEST

In order to validate the "REQ-080 – Operational temperature -20^0 to 60^{0}C", a TVAC test of a qualification model has been carried out. The antenna is placed in the central part of the TVAC baseplate, and it is surrounded by electromagnetic absorber.

The AUT is attached to the baseplate through the interface support shown in Figure 8 (copper part). Once the antenna-support-baseplate assembly was bolted, a total of 12 thermocouples were attached on the baseplate, the interface and the AUT.

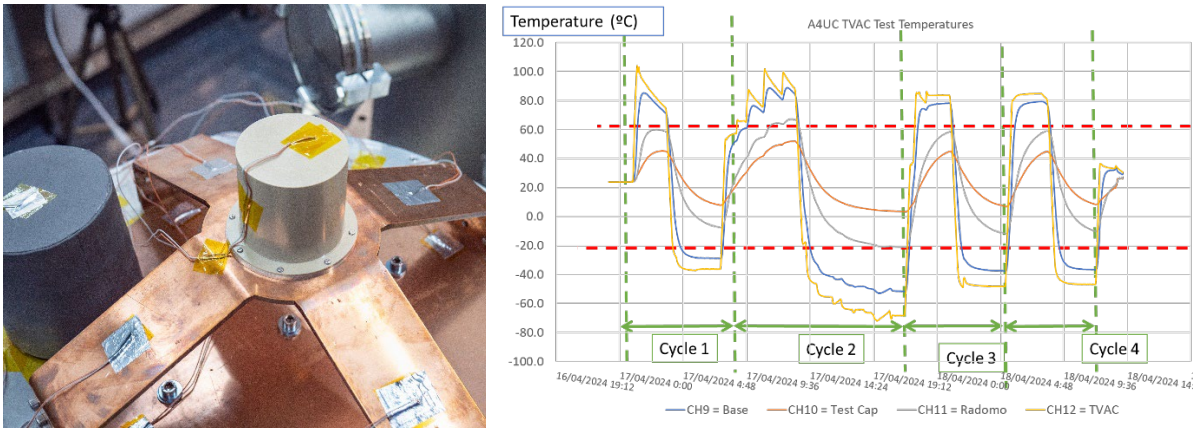

a) b)

Figure 14. a) Picture of the AUT and the test cap in the TVAC. b) ime evolution of main temperatures of the TVAC tests

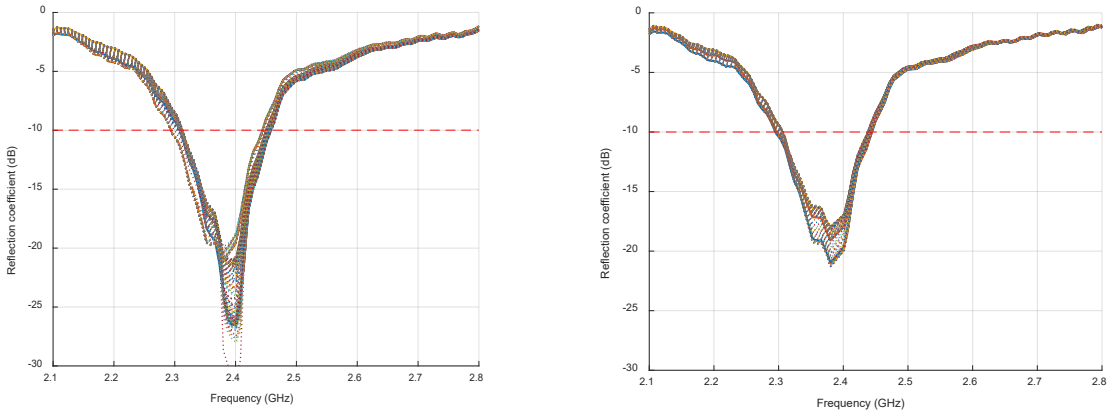

a) b)

Figure 15. Antenna reflection coefficient at first (a), and fourth (d) cycles

Four thermal cycles have been carried out, measuring the reflection coefficient every two minutes. The results are shown in Figure 15. In all cases, the minimum of the reflection coefficient remains at 2.4 GHz, with small variations. The antenna bandwidth remains at 150 MHz ± 10 MHz. The required bandwidth of this antenna is 100 MHz. In order to check the antenna performance after the TVAC test, the realized gain of the antenna was measured in the AC. The radiation pattern for some values of ϕ was measured moving θ which shows equivalent results to the ones obtained before TVAC test.

4.5 ANTENNA MEASUREMENTS IN RELEVANT SCENARIOS

Two different communications subsystems have been experimentally studied: one with only one port and a pagoda antenna, and a second one with 1x2 MIMO, using quasi-yagi (QY) antennas, with higher power consumption.

4.5.1 Measurements in Jameo de la Gente

A measure set was carried out in a skylight analogue ("Jameo de la Gente"). A QY antenna was placed on the top of the skylight and a set of points inside the skylight was selected, emulating a possible exploring mission. Only one orientation of the antennas was measured.

Figure 16. Top view of the measurement campaign in Jameo de la Gente.

The antenna pagoda was designed to enlarge a horizontal link and not specifically for this situation. Although its radiation pattern has a minimum in the vertical direction, the behavior of the pagoda antenna is comparable with the QY antenna. It has to take into account that the pagoda measures have an additional polarization loss of 3 dB.

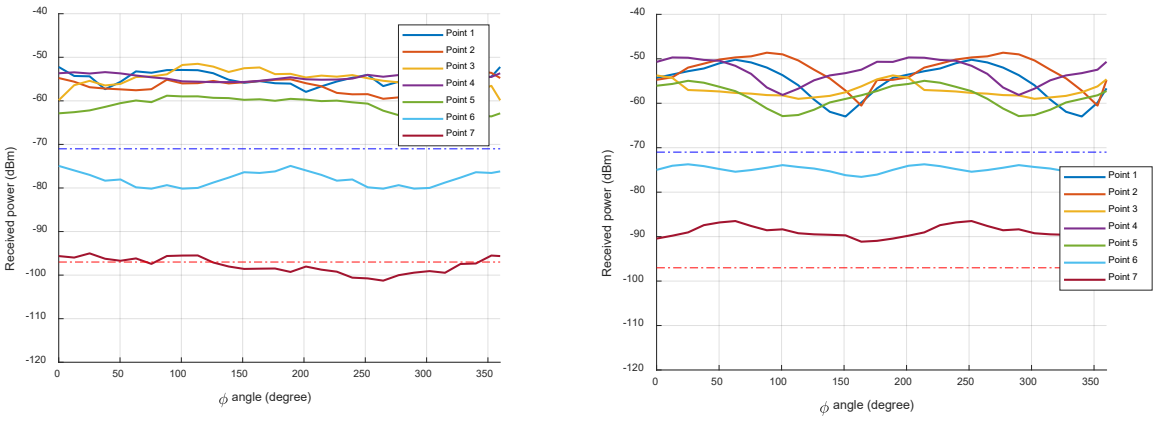

Figure 17. Received power sweeping the ϕ angle by the pagoda antenna (a) and the QY system (b).

4.5.2 Measurements in Los Naturalistas cave

In Los Naturalistas cave, the performance of the antennas has been measured in three different scenarios. The first scenario is a corridor with a bend. Eight positions have been selected. The first point is a simple point, used as reference. The other positions are points close to the walls and points without Line of Sight (LoS) (Fig. 18)

Selected points:

1. Center. 10.4m to Tx. LoS
2. Close to a wall. 15m to Tx. LoS
3. Close to a wall. 26m to Tx. LoS
4. Close to a wall. 31m to Tx. NLoS
5. Middle. 53m to Tx. NLoS
6. Middle. 65m to Tx. NLoS
7. On a boulder. 65m to Tx. NLoS
8. Behind a boulder. 65m to Tx. NLoS

Figure 18. Sketch of the measurement points in Scenario 1, in Los Naturalistas cave.

Fig. 19 shows the results obtained in this scenario. In general, the received power in the points with LoS is greater than -71 dBm. In the NLoS, the QY system has a small improvement, due to transmitter and receiver are antennas with better gain. The received power in the pagoda antenna remains practically constant, when the θ =0º. In the other orientation (θ =30º), some ripples appear due to the effect of fading. This effect is greater close to walls (points 2-4) and in NLoS points (4 -8). This effect is minor in the QY antennas because the circumference described by the phase center is smaller than in the case of the pagoda antenna.

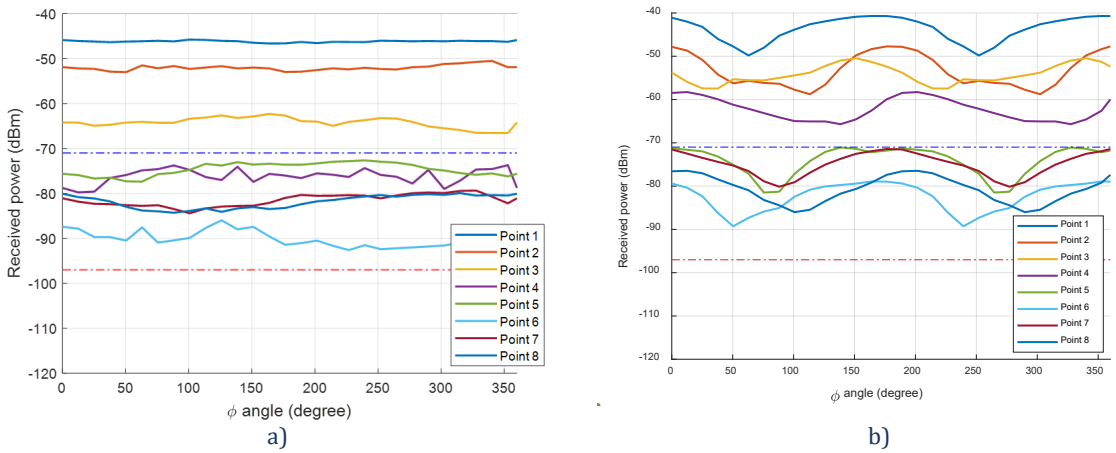

Figure 19. Received power sweeping the ϕ angle by the pagoda antenna (a) and the QY system (b) in scenario 1, in Los Naturalistas cave.

4.5.3 Measures in La Corona tube

Another set of measurement was carried out in La Corona tube. It is a narrower corridor, compared with both corridors in Los Naturalistas cave. This scenario has two bends that implies several points with NLoS.

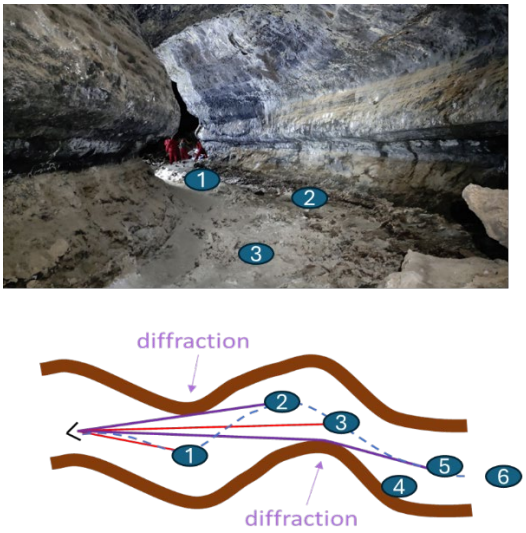

Selected points:

1. Center. 8.5m to Tx. LoS
2. Close to wall. 20m to Tx. LoS
3. Close to wall. 26m to Tx. NLoS
4. Middle. 31m to Tx. NLoS
5. Middle. 40m to Tx. NLoS
6. Middle. 49m to Tx. NLoS

Figure 20. Sketch of the measurement points in Scenario 3

The results between the two set of antennas are similar: the amplitude of the received signal diminish with the distance between transmitter and receiver, getting worse with NLoS situations. The behavior of the pagoda antenna is more stable than the one of the QY system.

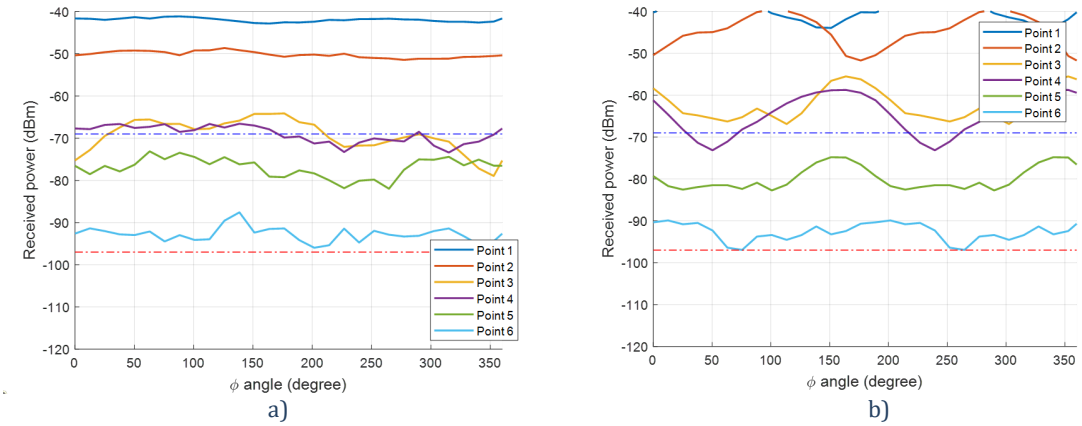

Figure 21. Received power sweeping the ϕ angle by the pagoda antenna (a) and the QY system (b) in scenario 3, in La Corona tube.